Design of high-performance photodiode receivers for optical tomography

Design of High-Performance Photodiode Receivers for Optical Tomography

Paul Wright, Krikor B. Ozanyan, Stephen J. Carey & Hugh McCann

***Abstract*—The design of instrumentation hardware for tomographic systems must take careful account of measurement noise. This is especially true in near-infrared absorption tomography, where the signal of interest is typically only a few percent of the total signal at the detector and the available optical power may have to be shared among many measurement channels.**

In this paper, the monitoring of photodiodes in near-IR absorption tomography is examined in detail but much of the material is applicable at wavelengths ranging from the UV to beyond 2.5 μm. The authors' application involves the frequency region 50 kHz to 2 MHz, which lies above that utilized in the majority of radiometric sensing systems, yet substantially below telecoms bit rates. The problem is further distinguished by the use of phase-sensitive detection schemes, which make local noise density more relevant than wideband noise performance and relax the requirement for DC precision.

Alternative transimpedance circuit configurations, including both single-ended and differential topologies, are analyzed with a view to optimization of signal to noise ratio (SNR). Typical values of photodiode capacitance and shunt resistance are shown to result in significant noise gain, greatly increasing the importance of amplifier voltage noise relative to other intrinsic noise sources. It is shown that, for applications of this type, viable alternatives to the traditionally dominant FET amplifier do exist. The relative susceptibility to coupled interference is also considered. The results of practical tests, involving class-leading operational amplifiers, are presented to support the analyses. These results also underline the need for careful circuit layout and shielding if the capabilities of these devices are to be fully exploited.

***Index Terms*—photodiodes, tomography, amplifier noise.**

I. Introduction

OPTICAL tomography is beginning to find application in both medicine and industry [1], [2]. Previous work at UMIST has demonstrated the considerable potential of near-infrared absorption tomography (NIRAT) as a tool for the study of hydrocarbon distribution in the cylinders of internal combustion engines prior to ignition. The present NIRAT system, illustrated schematically in Fig. 1, is a 32-beam hard-field tomograph operating at 1550 nm and 1700 nm wavelengths [3].

Currently, efforts are underway to increase the available frame rate to provide more detailed information at high engine rotation rates. Hindle [4] studied the impact of noise in the individual path concentration integrals on reconstruction accuracy and precision, and concluded that, although present SNR levels are adequate, little additional degradation can be tolerated. This constraint, in conjunction with the presently modest power output of commercially available solid-state sources at these wavelengths (1 mW to 5 mW) and the inherently weak absorption signals (less than 10% of optical throughput), makes a low-noise detection and amplification scheme vital to the success of this work. In the current system, around 3 μW (peak) of 1700 nm radiation arrives at each receiver, yielding a full-scale absorption signal equivalent to

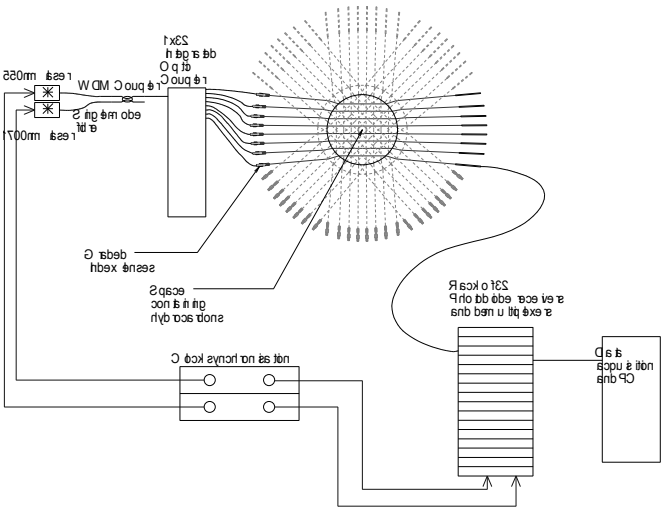

Fig. 1. Schematic representation of a 32-beam near-infrared absorption tomograph.

Manuscript received January 6, 2004. This work was supported by the U.K. Engineering & Physical Sciences Research Council (grant ref. GR/S05089) and by the U.K. Department of Trade and Industry, AOS Technology Ltd., Roush Technologies Ltd., and Ford UK Ltd., through their participation in the *IMAGER* project [www.imager].

H. McCann is with the Department of Electrical Engineering & Electronics, UMIST, Manchester, M60 1QD U.K.. (phone: +44 (0)161 200 4791; fax: +44 (0)161 200 4789; e-mail: h.mccann@umist.ac.uk).

P. Wright, K. B. Ozanyan, and S. J. Carey are with the Department of Electrical Engineering & Electronics, UMIST, Manchester, M60 1QD U.K.. (e-mail: p.wright-2@umist.ac.uk; k.ozanyan@umist.ac.uk; stephen.carey@ umist.ac.uk.)

All authors are members of the Virtual Centre for Industrial Process Tomography (VCIPT) [www.vcipt.org.uk].

150 nW, for typical conditions (stoichiometric air-fuel mixture at 10 bar and 125°C). Phase-sensitive detection (PSD) is already being used to aid signal recovery, so improvements must be made in the front-end optical and electronic systems preceding this.

The choice of sensor type is relatively straightforward; photodiodes offer unrivalled performance in applications of this kind. Depending upon the semiconductor chosen, they can be used from 300 nm to beyond 2.4 μm. They offer excellent linearity, good sensitivity and are far more robust, cheaper and easier to use than the photomultiplier tubes traditionally favored for low-level optical measurements. Most photodiodes represent a good approximation to an ideal current source and are normally used in conjunction with some form of current-to-voltage converter, most often a transimpedance amplifier (Fig. 2). It is in this front-end conversion/amplification process that the greatest scope for SNR improvement exists.

Various authors have considered photodiode monitoring (e.g. [5]) but the most comprehensive treatment of the topic is that of Graeme [6]. The extent of the latter work only serves to underline the surprising complexity of the problem. Much of the published material addresses one of two distinct domains; low-frequency sensing applications, requiring good precision, or telecommunications receivers, with bandwidths usually in excess of 10 MHz. The tomographic application typically lies between these two extremes of frequency. It is further distinguished by the use of phase-sensitive detection, which reduces the required DC precision and alters the relative importance of the various noise mechanisms, as discussed in Section II.

The high feedback resistances, that are typically necessary in photodiode amplifiers, have traditionally pushed designers towards the use of FET-input amplifiers, with their ultra-low bias currents, to achieve acceptable DC performance. Indeed, some of Graeme's analyses presume the use of FET amplifiers from the outset, allowing amplifier current noise to be considered negligible. The authors will show that in the tomographic case, at least, other approaches do merit consideration when SNR is paramount.

Common current-to-voltage converter circuits are examined in Section II. The merits of the various configurations are considered with particular regard to signal bandwidth and the noise mechanisms present in each case. Section III compares predicted and measured performance, assuming realistic photodiode parameters, and highlights the importance of layout and shielding in realizing the capabilities of state-of-the-art operational amplifiers in this application.

II. Circuit Analyses

A. Overview

The classic transimpedance amplifier is the most widely used arrangement for high-sensitivity (zero-bias) photodiode monitoring, and is discussed in part B. A differential alternative, based upon the instrumentation amplifier topology, is examined in part C. For each of these two circuits, the signal bandwidth is considered and then five intrinsic noise mechanisms are examined; detector shot noise, detector Johnson noise, amplifier current noise, feedback Johnson noise and amplifier voltage noise. (Throughout this paper, these five terms are used either to denote the input-referred noise contribution of the mechanism in question, or to refer in abstract terms to that mechanism. All noise processes are considered in terms of spectral density.) Part D considers the resistive-tee feedback arrangement sometimes used in circuits of this type. Finally, a simpler, single op-amp, differential configuration is discussed in part E.

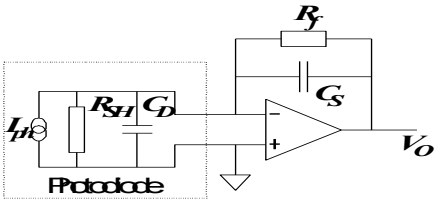

Fig. 2. Classic transimpedance amplifier. An expanded representation of the photodiode with explicit photocurrent source I_{ph}, shunt resistance R_{SH}, and diode capacitance C_D is shown. For simplicity, this representation is replaced in subsequent figures by a standard diode symbol.

B. Classic Transimpedance Amplifier (TIA)

Consisting of a single operational amplifier and feedback resistor, the latter possibly shunted by a capacitor for bandwidth limitation or gain stabilization, the simplicity of this circuit (Fig. 2) belies its effectiveness. Given a suitably fast operational amplifier, the transimpedance gain will be rolled off by the combination of stray and supplemental (if any) capacitance C_S. Controlled gain peaking may be used to extend the useful bandwidth, in which case the gain *and* phase responses of the amplifier must be carefully considered. The signal (transimpedance) gain, for an operational amplifier of open-loop gain A_{OL}, is then given by

$$A_{SIG} = \frac{V_O}{I_{ph}} = \frac{-A_{OL}}{\frac{1+A_{OL}}{Z_f} + \frac{1}{Z_i}} \quad , \tag{1}$$

where

$$Z_f = R_f \parallel C_S \tag{2}$$

and

$$Z_i = R_{SH} \parallel C_D \parallel Z_A \tag{3}$$

represent the complex feedback and input impedances respectively. In many cases, the differential input impedance of the amplifier,

$$Z_A = R_{AMP} \parallel C_{AMP} \quad , \tag{4}$$

will not produce a significant change in Z_i but it can be important when considering small area photodiodes or amplifiers with bipolar input stages. The contributions of the five noise mechanisms are summarized in Table I. The RMS noise sum is often dominated by only one or two of these terms. Detector shot noise, detector Johnson noise and amplifier current noise all see the signal gain of the amplifier so SNR improvement can only be effected by addressing the multiplying factor in each case. For example, shot noise in the detector increases as the square root of the signal photocurrent I_{ph}, whereas signal output increases in direct proportion to the photocurrent. In a system where detector shot noise is dominant, SNR can only be improved by increasing the signal photocurrent. Similarly, detector Johnson noise can be reduced only by cooling the photodiode or by use of a higher shunt resistance detector. This term assumes great significance in mid-infrared systems, where detector shunt resistances tend to be much lower, but only constitutes around 0.5% of the total noise in the NIRAT system. The contribution arising from amplifier current noise is wholly determined by the properties of the amplifier selected. The use of a low bias current, usually FET-input, part will often render this term insignificant (the shot noise of the bias current is one contribution to amplifier current noise).

TABLE I

NOISE CONTRIBUTIONS AT THE OUTPUT OF A CLASSIC TRANSIMPEDANCE AMPLIFIER

Noise Mechanism	Contribution at Output
Detector shot noise	$\sqrt{2qI_{ph}} \cdot A_{SIG}$
Detector Johnson noise	$\sqrt{4kT/R_{SH}} \cdot A_{SIG}$
Amplifier current noise	$i_n \cdot A_{SIG}$
Feedback Johnson noise	$\sqrt{4kTR_f}$
Amplifier voltage noise	$e_n \cdot A_{ne}$

Where $q = 1.6 \times 10^{-19}$ C is the electronic charge, the Boltzmann constant $k = 1.38 \times 10^{-23}$ J·K^{-1}, T is the thermodynamic temperature (kelvin), and i_n (A/$\sqrt{\text{Hz}}$) and e_n (V/$\sqrt{\text{Hz}}$) are, respectively, the input current and voltage noise densities of the operational amplifier.

Given adequate open-loop gain, the Johnson noise of the feedback resistor appears directly at the output and, unlike the preceding three terms, does not see the signal gain of the amplifier. For signals within the bandwidth of the current-to-voltage converter, however, SNR will improve as the square root of R_f, leading to the selection of high values of feedback resistance, limited primarily by DC performance considerations.

Amplifier voltage noise makes the most complex, and often most significant, contribution to the total output noise. The input referred voltage noise of the operational amplifier is multiplied by the circuit's noise gain A_{ne} (the reciprocal of the feedback fraction), rather than the signal gain A_{SIG},

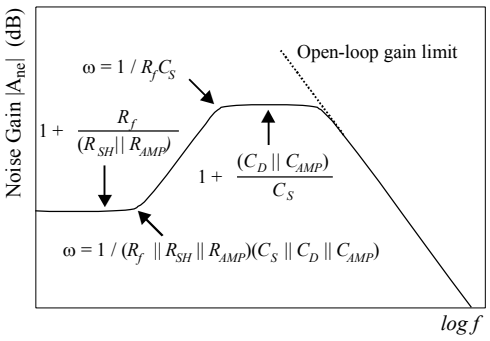

Fig. 3. Noise gain of the transimpedance amplifier.

$$A_{ne} = \frac{1 + R_f / \left(R_{SH} \parallel R_{AMP} \right) + R_f \left(C_D \parallel C_{AMP} \parallel C_S \right) s}{1 + R_f C_S s} \quad . \tag{5}$$

This can increase the relative contribution of this noise source by several orders of magnitude when monitoring large-area (high capacitance) photodiodes. The form of the noise gain is shown in Fig. 3. The logarithmic frequency scale used places undue emphasis on the low-frequency region; it is important to appreciate that the *vast majority* of the amplifier's bandwidth is affected by noise gain peaking. Note also that the noise gain in the plateau region is a function only of the circuit capacitances; it is independent of R_f. It may seem appealing to reduce the modulation frequencies employed in the phase-sensitive detection scheme to avoid this noise gain peak. However, analysis reveals that achieving this, whilst remaining above the 1/f noise corner, places severe restrictions on the signal bandwidth available after demodulation.

C. Fully Differential I-V Converter

The circuit of Fig. 4 is closely related to the three op-amp instrumentation amplifier but is more readily understood as a pair of classic TIA's followed by a differential amplifier. This topology is intended to exhibit improved rejection of common-mode interfering signals, as compared to single-ended circuit arrangements. Its performance has much in common with the classic TIA but subtle differences do exist. For a given transimpedance gain, the differential configuration allows each individual feedback resistor to provide half of the total resistance requirement. Assuming the stray capacitance remains unchanged, increased bandwidth will result. This split configuration does impact on noise performance, however. Amplifier voltage noise is effectively increased by 3dB at all frequencies, compared to the classic TIA. Amplifier current noise is reduced by 3dB at low frequencies but increased by 3dB above the R_fC_S pole. In practice, the region of greatest interest often lies near to or just below this pole so the current noise situation may be marginally improved.

An arguably more significant feature of the differential

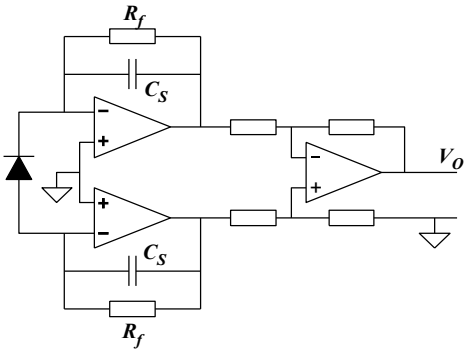

Fig. 4. Fully differential I-V converter. The amplifiers' input capacitances and resistances are not shown explicitly.

configuration is its ability to reject interfering signals. With careful layout, a highly symmetric input stage can be realized, giving excellent scope for common mode rejection in the following amplifier. In some instances this will outweigh intrinsic noise considerations. Although it is possible to implement this circuit using a monolithic instrumentation amplifier, the values of feedback resistance used in commercial parts (<10kΩ) are inappropriate for most photodiode monitoring applications, making construction of two discrete classic TIA's necessary. Careful matching is necessary to maintain good common mode rejection performance but will also improve DC precision as some cancellation of offsets will occur.

D. Resistive-Tee Feedback Network

Rather than being a circuit in its own right, this is a modification that can be applied to the feedback network of the classic or differential transimpedance circuits described

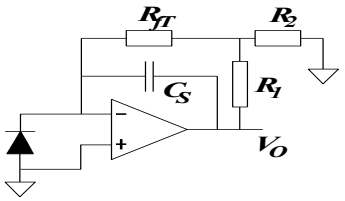

Fig. 5. Resistive-tee feedback arrangement applied to a classic TIA.

above. Fig. 5 shows its application to a classic TIA. The replacement of the high-value feedback resistor with a resistive tee-network allows the synthesis of very high equivalent feedback resistances but has a, partly justified, reputation for poor noise performance [6]. In this circuit R_1 and R_2 form a voltage divider that presents a fraction of the output voltage to R_{fT}. Provided R_1 and R_2 are small compared to R_{fT}, the effective feedback resistance R_{feq}, defining the transimpedance gain, is given by

$$R_{feq} \approx R_{fT}\left(1 + R_1/R_2\right). \tag{5}$$

This allows high effective feedback resistances to be realized using relatively small values of resistance. This is especially useful in high bandwidth, high gain, systems that would otherwise be limited by the action of stray capacitance on R_f. A further benefit of the tee-network is a reduction in the output offset arising from the amplifier's bias current requirement by a factor of $1 + R_1/R_2$, albeit at the expense of a proportional increase in the output error resulting from amplifier offset voltage.

The noise performance of the tee-network can be a cause for concern. The noise mechanisms are essentially identical to those encountered in the classic TIA. For a given level of transimpedance gain, the contributions of detector shot noise, detector Johnson noise and amplifier current noise will be equal to those found in the classic TIA. The low-value resistors R_1 and R_2 do not add significant Johnson noise. The action of the tee-network applies a scaling of $1 + R_1/R_2$ to the noise of R_{fT} but this is partly offset by the reduced value of this resistor compared to the R_f required for a given transimpedance gain. Overall, the feedback network contribution to the output noise will be $(1 + R_1/R_2)^{0.5}$ times greater than in an equivalent classic TIA. For modest values of R_1/R_2 this increase may not lead to a significant change in the total RMS noise if other mechanisms remain dominant.

The noise gain, and therefore the amplifier voltage noise contribution, of the resistive-tee is subtly different to that of the classic TIA. In the low frequency limit, an increase in the noise gain has indeed occurred. This is accompanied, however, by an increase in the frequency at which the onset of gain peaking occurs (the zero formed by the action of $(C_D \parallel C_{AMP} \parallel C_S)$ on R_{fT}). Far more significant is the high frequency region of the noise gain curve, which is identical to that of the classic TIA; in the high frequency limit we have $1 + (C_D \parallel C_{AMP})/C_S$ as before. Overall, the adoption of the resistive-tee feedback network will only incur a significant noise penalty if it brings feedback Johnson noise to prominence.

E. Simple Differential I-V Converter

It is possible to implement a differential transimpedance amplifier using a single operational amplifier (Fig. 6.) but this approach does have some limitations. Unlike the preceding circuit, there is a significant signal swing at the amplifier inputs. This brings the common mode capacitance at the amplifier input C_{CM} into play. This may be much larger than

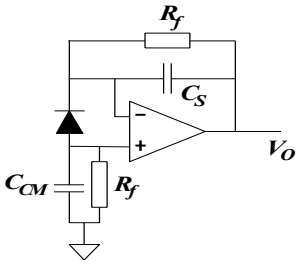

Fig. 6. 'Simple' differential I-V converter

the differential input capacitance, particularly if the photodiode can is grounded for shielding purposes, and may therefore reduce the available bandwidth. This topology does, however, allow the designer to access the advantages of a differential scheme without significant extra layout complexity or component cost, at least in low-frequency applications. This circuit was considered inappropriate for our application and was not investigated further.

III. Practical Performance Measurements

A. Overview

It is apparent from the preceding analyses that, in the absence of coupled interference, the classic TIA (with resistive-tee feedback if appropriate) would be expected to perform better than the differential configuration, from a noise perspective. In practice, it is therefore necessary to consider the relative importance of intrinsic noise and external interference when selecting a circuit configuration.

In the present study, the circuits of Fig. 2 and Fig. 4 were implemented and their performance compared to the results of modeling. The photodiode chosen (G8421, Hamamatsu Photonics; $R_{SH} \approx 1.5$ MΩ, $C_D \approx 70$ pF) was a 1.9 μm-cutoff extended InGaAs device. Three alternative operational amplifiers were tested. The first of these, the OPA655 (Texas Instruments), was chosen to epitomize the traditional approach to wideband photodiode monitoring. It features an FET input, giving negligible bias current and current noise. The second amplifier selected (AD8057, Analog Devices) has similar bandwidth and voltage noise performance to the OPA655 but with the bias current, current noise and input impedance of a bipolar part. Despite the increased current noise, modeling predicts that amplifier voltage noise will be most significant for the AD8057. The third amplifier chosen (THS4031, Texas Instruments) was expected to show a shift from voltage noise to current noise dominance but is otherwise very similar to the AD8057. The THS4031 has less phase margin than the OPA655 and was expected to show appreciable signal gain peaking. The increased bias currents of the AD8057 and THS4031 are acceptable, subject to dynamic range limits, thanks to the PSD scheme that will be employed. The relaxed DC performance requirement allows bipolar devices, with their generally lower levels of amplifier voltage noise, to be considered.

The circuits were all implemented using surface mount components and careful layout to maintain low inductance. The amplifier under test was followed by a unity gain voltage buffer (BUF634, Texas Instruments), to isolate the circuit from the effects of test equipment and cable loading, except for the purposes of DC offset measurement. A 54622A digital oscilloscope (Agilent Technologies) was used to measure the output voltages. The signal bandwidth was characterized using an 880 nm LED-based light source, which could be modulated at up to 20 MHz. Noise performance was assessed by blanking the photodiode and performing a spectral analysis of the output noise voltage. Table II compares predicted and measured performance for the various combinations of circuit topology, amplifier and shielding.

No extensive work was done on resistive-tee variants as no SNR improvement was expected to result from the adoption of such an arrangement and the transimpedance values required in the present application were amenable to single-resistor implementation. Preliminary noise density measurements supported this view.

B. Signal Bandwidth

The majority of the measured –3dB bandwidths exceed the

TABLE II

Predicted & Measured Performance of Classic & Differential TIA's

------- Configuration -------		---------- Predicted ----------				---------- Measured ----------				
Circuit topology	Amplifier	f_{-3dB} (kHz)	Output noise density (μV/√Hz)	SGNDR (√Hz/nA)	Dominant noise power sources (% total noise power)	f_{-3dB} (kHz)	Shielded output noise density[1] (μV/√Hz)	Shielded SGNDR[2] (√Hz/nA)	Unshielded output noise density[1] (μV/√Hz)	Unshielded SGNDR[2] (√Hz/nA)
Classic TIA	OPA655	320	1.2	680	AVN (72%); DSN (25%)	350	0.7	1285	8.3	108
	AD8057	290	1.3	580	AVN (65%); ACN (17%); DSN (17%)	590	1.8	750	4.3	314
	THS4031	440	1.5	680	ACN (70%); DSN (23%)	605	1.3	1154	4.7	319
Differential	OPA655	670	1.9	760	AVN (84%); DSN (15%)	645	1.0	1500	1.4	1071
	AD8057	625	2.1	650	AVN (79%); ACN (10%); DSN (10%)	895	2.3	652	2.9	517
	THS4031	760	1.7	1020	ACN (67%); DSN (22%);AVN (10%)	1440	1.3	1154	1.4	1071

All models use $C_D = 70$ pF, $R_{SH} = 1.5$ MΩ, $I_{ph} = 1.5$ μA, $C_S = 0.35$ pF
Classic TIA – $R_f = 1.5$ MΩ; Differential – $R_f = 750$ kΩ
AVN – amplifier voltage noise ACN – amplifier current noise DSN – detector shot noise.

[1] Measured at 440 kHz with no radiation incident on photodiode.
[2] Measured SGNDR taken as the ratio of measured signal gain to measured (no incident radiation) output noise density at 440 kHz.

predicted values. Although the actual stray capacitance may have been somewhat less than the 0.35 pF assumed for modeling purposes, as might be expected given the 'tight' layout and surface-mount construction, the unexpectedly large bandwidths seen from the AD8057 and THS4031 cannot be attributed to stray capacitance reduction alone. Both amplifiers show greater gain peaking than anticipated, indicating deficiencies in their assumed open loop responses. Modest amounts of gain peaking can offer useful bandwidth extension but should be used with care, to avoid undesirable instability. Note, however, that no improvement in SNR will generally result, as the same gain increase will be applied to most of the noise terms.

C. *Intrinsic Noise Performance*

Signal gain to noise density ratios (SGNDR's) are used in Table II to allow comparison of noise performance under 'standardized' conditions, irrespective of the *actual* signal gain of the TIA under consideration. This was preferred to the use of the SNR resulting from some arbitrary bandwidth. In the absence of shielding, coupled interference makes a dominant (and variable) contribution to the output noise of the single-ended circuit, obscuring the effects of the intrinsic mechanisms. The shielded measurements, however, show good agreement with theory. The best *measured* performance obtained from a classic TIA in these tests (1.1 μV/√Hz) is substantially better than even the *theoretical* performance limit of our previous system (10 μV/√Hz).

Results with the differential topology are also encouraging. Intrinsic noise levels generally no more than 3-4dB above those of the corresponding single-ended circuits have been observed.

D. *Susceptibility to Coupled Interference*

Two methods were used to compare the performance of the single-ended and differential topologies in this regard. The first, a passive test, examined the increase in output noise observed when electromagnetic shielding was removed. The single-ended circuit showed typically a four-fold increase in measured noise, even in a relatively 'quiet' electronic environment, whereas the increase in the differential case was only 16%. The obvious limitation of this experiment is the uncontrolled nature of the interference sources and their coupling. A second study was therefore performed, in which a 440 kHz signal was applied, via coupling capacitors, to both terminals of the photodiode. Differential and classic TIA's, both of transimpedance gain 1.5×10^6 V/A, were compared, using an input signal of magnitude 100 mV rms and coupling capacitors of 7 pF. The differential topology showed good rejection of this common-mode input; the 440 kHz component of the output being only 180 mV rms. In contrast, the single-ended circuit had a 440 kHz output component of 2.5 V rms. The marked reduction (23 dB) in susceptibility to coupled interference that the differential approach offers may be invaluable in harsh electronic environments.

IV. Conclusion

Selection of a near-optimal amplification scheme for photodiode monitoring has been shown to be far more involved than superficial analysis would suggest. In fact, the dependence of amplifier performance on the capacitance and shunt resistance of the detector dictates that the photodiode and amplifier should be considered as an integrated system from the outset. Only by taking full account of the properties of the photodiode in question can the most appropriate solution be selected. The performance of the circuits discussed in this paper has many subtleties. Note, for instance, that the fastest operational amplifier tested (OPA655, f_C = 400 MHz) yields the smallest –3dB bandwidth, as it produces less gain peaking than the slower amplifiers.

Optimizing the SNR performance of these circuits must involve careful assessment of the relative importance of intrinsic noise and coupled interference. Where the former dominates, the classic TIA is unsurpassed. The resistive-tee affords extra design flexibility, particularly when high transimpedance gain is required, and if used appropriately incurs a minimal noise penalty. Coupled interference is better addressed using a differential configuration, at the expense of a possible increase in intrinsic noise. It is worth noting, though, that this increase may not be significant in current noise dominated circuits.

The excellent performance of the OPA655 in these tests underlines the strength of the traditional FET-input amplifier in this application. However, even though the OPA655's input-referred voltage noise is class-leading (6 nV/√Hz), the resulting TIA is amplifier voltage noise limited. If, as in our case, the DC performance requirement can be relaxed, the designer can consider a number of bipolar parts that offer improved voltage noise performance. This may permit a better balance to be struck between voltage and current noise, leading to a reduction in the total RMS noise.

The difficulties of realizing theoretical performance levels should not be underestimated. It is hard to obtain precise values for several of the model parameters, particularly stray capacitances. Even where the model does provide an accurate representation of potential performance, it may not be possible to shield the system adequately from coupled interference. The unknown and variable nature of the interfering signals means that testing can only ever provide indicative performance levels. If high levels of interference are anticipated, a differential topology may be preferable, despite its generally higher intrinsic noise.

The benefits of this optimization process are evident. A clear understanding of the noise mechanisms permits informed decisions to be made regarding circuit topology and design, amplifier type and detector. In the authors' application, this has made possible a reduction of more than 20 dB in measured output noise density in what was already a carefully-designed low-noise system (15 μV/√Hz). In some cases, even greater gains may be possible.

Despite the authors' efforts the system does not quite

achieve shot-noise-limited performance, although it is very close to not only that limit but also those imposed by the various optical noise mechanisms present. More importantly, the nature of the limitations is well-understood, ensuring that amplifiers or detectors which have the potential to move the system still closer to the global intrinsic noise minimum can be readily identified. To achieve an equivalent improvement in SNR by increasing the available optical power would have cost in the region of US$ 100,000 and added significantly to the complexity of the system. Given such significant technical and economic advantages, the effort expended on optimization seems wholly justified.

REFERENCES

[1] J.C. Hebden, A. Gibson, R.M. Yusof, N. Everdell, E.M.C. Hillman, D.T. Delpy, S.R. Arridge, T. Austin, J.H. Meek, and J.S. Wyatt, "Three-dimensional optical tomography of the premature infant brain," Phys. Med. Biol., 47 4155-4166, 2002

[2] H. Philip, A. Plimon, A. Hirsch, G. Fraidl, and Winklhofer, E., "A Tomographic Camera System for Combustion Diagnostics in SI engines," SAE95068, 1995

[3] F.P. Hindle, S.J. Carey, K.B. Ozanyan, D.E. Winterbone, E. Clough, and H. McCann, "Measurement of Gaseous Hydrocarbon Distribution by a Near-Infra-Red Absorption Tomography System," Journal of Electronic Imaging, 10, 593-600, 2001

[4] F.P. Hindle, "Absorption and Fluorescence Tomography for Hydrocarbon Distribution Measurement in Internal Combustion Engines," Ph.D. Thesis, Dept. Elect. Eng. & Electronics, UMIST, U.K., 2001

[5] B.C. Baker, "Comparison of Noise Performance Between a FET Transimpedance Amplifier and a Switched Integrator," Burr-Brown Application Note, 1993

[6] J. Graeme, *Photodiode Amplifiers – Op Amp Solutions*. McGraw-Hill, 1995

Paul Wright was born in Durham, U.K. in 1972 and was awarded the B.Sc.(Hons.) in pure & applied physics from the University of Nottingham, U.K. in 1993 and the Ph.D. in physics from the University of Exeter, U.K. in 1997.

Following his Ph.D., he worked as a LECTURER in the Division of Measurement & Control at the University of Teesside before spending five years with Land Infrared as a PROJECT ENGINEER working on industrial applications of optical thermometry. He joined UMIST (Manchester, U.K.) in 2002 as a RESEARCH ASSOCIATE.

Krikor B. Ozanyan (M'95-SM'03) received his MSc degree in engineering physics (semiconductors) and PhD degree in solid-state physics in 1980 and 1989 respectively, from the University of Sofia, Bulgaria. With a strong background in experimental semiconductor physics, applied optics and spectroscopy, he has held research and academic posts in the University of Sofia, The Norwegian Institute of Technology (Trondheim, Norway), the University of Hull (UK), and the University of Sheffield (UK), working on projects ranging from Brewster-angle mid-IR spectroscopic ellipsometry and electron confinement in quantum barriers, to the demonstration of the lasing at 333nm from strained MQW ZnCdS/ZnS structures and in-situ real-time optical monitoring of growth of III-V semiconductors in MBE and MOCVD machines. His current interests are in the area of optical sensing and indirect imaging by optical modalities, signal processing for optical experiments, and spectroscopy with ultrafast laser sources. Dr. Ozanyan has been a Member of the Institute of Physics (UK) since 1995.

Stephen Carey received his B.Eng. degree in electronic engineering from the University of Bristol in 1987, and MSc (1988) in microwaves and modern optics from University College London. After a period in industry with Sifam (Torquay, UK) and Bookham Technology (UK), developing equipment for opto-electronic device production and reliability assessment, he joined UMIST in Manchester. At UMIST he developed hardware for the spatial location of hydrocarbons by near-infrared tomography, receiving a PhD in 2001.

Prof. Hugh McCann (M'03) was appointed PROFESSOR OF INDUSTRIAL TOMOGRAPHY at UMIST in 1996, and was Head of the Dept. of Electrical Engineering & Electronics (1999-2002). Graduated from the University of Glasgow with B.Sc. in Physics (1976) and PhD (1980). After 10 years' experience in High Energy Particle Physics (Glasgow, Manchester, CERN and DESY), McCann worked in industrial R&D for 10 years at the Royal Dutch/Shell Group's Thornton Research Centre, where his research topics included explosions hazards and turbulent combustion, *in-situ* engine measurement technology and lubricant product formulation. His work was recognized by the SAE Arch T. Colwell Award in 1995. Throughout his career, McCann has been deeply involved in measurement technique development, with heavy emphasis on multi-dimensional techniques. A Member of the Institute of Physics (UK) since 1987, he was elected Fellow of the IEE in 2000. He is Chairman of U.K. Professors & Heads of Electrical Engineering (2003-). He is author/co-author of over 80 publications in international refereed journals.